SCA2003-24: NMR IMAGING WITH DIFFUSION AND RELAXATION

Boqin Sun, Keh-Jim Dunn, Gerald A LaTorraca*, and Donald M Wilson*
ChevronTexaco Exploration and Production Company

This paper was prepared for presentation at the International Symposium of the Society of Core Analysts held in Pau, France, 21-24 September 2003

ABSTRACT

We developed novel NMR imaging techniques which can be used to characterize fluid distribution and pore sizes in rock samples. The combination of imaging with relaxometry not only provides the proton population map in core samples but also incorporates information about the relaxation times and diffusion coefficients of pore fluids in a rock sample. NMR images of a core plug sample were obtained where the proton signal was successively encoded with information on relaxation time and diffusion coefficient of the pore fluids. The encoding was achieved by imposing a saturation recovery sequence for T1 relaxation, or a Tanner (or similar) sequence for the diffusion coefficient, before the imaging pulsing sequences. Thus, the NMR images were processed to yield the normal proton population image with an extra dimension showing either the relaxation time or the diffusion coefficient distributions. This procedure allows us to identify how the fluid is distributed within the core plug using the contrast in the diffusion coefficients, as well as the characteristics of the pore fabric using the T1 relaxation time distribution. It also provides a means of inferring the surface wettability in the spatial image of a core plug. Several experimental examples will be presented to illustrate the techniques.

INTRODUCTION

Petrophysical applications of NMR imaging of core samples started in the mid 1980s. The main focus was on obtaining high-resolution NMR imagings of porosity and saturation distributions in rock samples [1]. A variety of magnetic resonance imaging (MRI) techniques has been applied to determine the petrophysical properties of porous media. For example, porosity and saturation distributions of fluids in a rock sample can be elicited with MRI imagings [2-4]. MRI has also been applied to monitor fluid displacement (or movement) [5-8], wettability effects on oil-water configurations [9], and oil recovery [10, 11], to assess formation damage [12, 13], and to provide the petrophysical properties of complex carbonates [14].

We present here a new method of NMR core-plug imaging which also provides information on distribution of T1 relaxation times, or diffusion coefficients of fluids in rock samples at pixel level. Based on the current technology, it is still very difficult to obtain rock imaging at the pore size scale for most sandstone rock samples. The major limitation comes from strength of both

external field gradient and internal field gradient in pores [15]. The external field gradient is normally in the range of few 10s of gauss and limited by the current state of the technology and the size of the sample. However, the internal gradient field caused by the susceptibility contrast between grains and fluids is proportional to the static field applied to the sample and can range from zero to a few hundred gauss [16]. Internal field gradients broaden the resonance lines and reduce our ability to use frequency coding, as created by the external gradient, to distinguish spatially allocated fluids. In other words, the existence of internal field gradients reduces the spatial resolution of MRI and limits the application of MRI techniques to analyze core samples. Thus, MRI by itself can only provide fluid distributions inside cores, but fails to elicit the wettabilities and pore size distributions. However, T1/T2 relaxation times and diffusion coefficients have been successfully used to characterize pore size distributions and the viscosities of fluids in formations from both logging and core analysis [17]. Ideally then, a NMR image combined with a relaxometry measurement can yield the normal proton population image with an extra dimension showing either the relaxation time or the diffusion coefficient distributions. We present experimental results of a test sample and real rock samples measured by MRI combined with T1 measurements and diffusion measurements.

EXPERIMENTAL SETUP

Our NMR imaging system includes a wide bore vertical magnet from Bruker, an MSL 200 Bruker spectrometer upgraded by Resonance Instrument, a Doty microimaging probe, and Techron gradient power amplifiers. The magnetic field was set at 85 MHz as a compromise between the higher S/N ratio achieved at higher fields and the reduced susceptibility broadening encountered at lower fields.

Figure 1 shows the 1D version of T1 inversion-recovery MRI (T1MRI) pulse sequence. Following the typical convention of the magnetic frame of reference, the magnetization is inverted to the negative z-axis by the first 180° pulse and starts to recover during the following delay time t_1 (also referred to as recovery time). The partially recovered magnetization is then tipped to the xy-plane by a hard 90° pulse and starts to precess around the static magnetic field. During the precession, a gradient pulse is applied to encode the spatial position to individual spins. After encoding, a 180° pulse is applied to form an echo for detection. During the echo acquisition period a readout gradient is applied. By varying the recovery time between the first 180° and 90° pulses, one is able to obtain a T1 recovery curve for every spatial position along the z-axis. After acquiring a set of echoes with different recovery times, we then performed a FFT (Fast Fourier Transform) and a BRD (Butler, Reeds, and Dawson) [18] inversion to obtain a 3D correlation map: The first dimension is spatial position, the second dimension is T1 relaxation time, and the third dimension is the proton population at a given spatial position and T1 relaxation time.

Figure 2 shows the 2D version of a T1MRI pulse sequence. After the T1 encoding, a soft 90° pulse and a z-gradient pulse are simultaneously applied to select a xy slice. Following a standard 2D MRI procedure, a 2D data set was acquired and each data set encoded with different x and

y gradients. A 2D FFT and a BRD inversion results in a correlation map between the T1 distribution and 2D porosity profile for the selected xy slice.

Figure 3 shows the 1D version of a diffusion MRI (DMRI) pulse sequence. This sequence is similar to the 1D T1MRI except that the inversion-recovery part has been replaced by the Tanner stimulated echo sequence [19]. The diffusion effects can be seen by varying either the delay time between the second and third 90° pulse, or the gradients applied during the Tanner sequence. In our experiment, the gradients were varied. In a standard Tanner sequence, the stimulated echo is acquired directly after the third 90° pulse. For our pulse sequence, in order to obtain 1D porosity profile, an echo sequence with gradient encoding and decoding pulses was initiated after the Tanner sequence. FFT and BRD inversions result in the correlation map of diffusion coefficient and 1D porosity profile, along the z-axis.

RESULTS AND DISCUSSION

T1 Measurement with 1D Imaging

To illustrate 1D T1MRI, we prepared a three-cell sample arranged vertically in a test tube. The first cell was filled with distilled water (with the T1 relaxation time of 3s at room temperature), the second, with crude oil (with T1 of 200ms at room temperature), and the third, with doped water (with T1 of 10ms at room temperature).

In the 1D T1MRI experiment, the 90° RF pulse length was 33μs and 180° RF pulse was 67μs. The recovery time varied from 0.1ms to 10s according to the following order: 0.1ms 0.3ms, 1ms, 3ms, 10ms, 30ms, 100ms, 300ms, 1s, and 10s. The wait-time between two scans was 5s. The gradient pulse length was 300μs and the readout gradient pulse length was 600μs. The gradient strength was 7gauss/cm and the dwell time in the acquisition was 1μs. The echo spacing was 1ms and 512 data points were acquired. Note that it is important to have long enough delay time between the first gradient pulse and the second 180° pulse in order to obtain an undistorted 1D imaging profile. At the beginning of the development, we used 20μs and later found it should have been 300μs or longer.

Once the complete echo was acquired, we performed a FFT to obtain a spectrum whose intensity was a T1 encoded hydrogen population profile along the applied gradient direction (in this case it is axial). Note that due to the applied gradient, the phase of the FFT spectrum is linearly proportional to the frequency. We can perform either a linear phase correction or just simply use the amplitude. For N different recovery times, we obtain N T1-encoded spectra. If we arrange all the spectra along the recovery time, for each frequency component we have a T1 recovery curve. Performing a T1 inversion on the T1 recovery curves results in a 3D map whose first axis is frequency (or axial position), the second axis is T1 relaxation time, and the third axis is the hydrogen intensity at given axial position and T1 relaxation time. Figure 4 shows a 1D T1MRI correlation map of three different fluids.

From the frequency/axial domain, we clearly see three different cells and the length of each cell is about 2cm. In the T1 relaxation time domain, three different relaxation times are observed: for the distilled water, about 3s, for the crude oil, about 200ms, and for the doped water, around 20ms. Note that the intensity profiles of two cells at their ends are not flat due to end effects from the gradient coil.

After a core-flood experiment, one usually wants to know how the original fluid was displaced by the flood along the axial direction. Traditionally we need to run a 3D MRI imaging on the flooded core plug to see the fluid distribution. Such an experiment usually takes a long time to run. Furthermore, in many cases, it is also very difficult to distinguish the original fluid in the core with the flooding fluid by MRI alone. The 1D T1MRI gives a quick and reliable way to monitor the fluid displacement in a core-flood experiment. It is quick because we only need to take a few 1D images. The reliability comes from the fact that the T1 relaxation time is highly variable in fluids. The T1 distribution also allows monitoring the free fluid and BVI in core samples. Figure 5 shows an example of 1D T1MRI with two water saturated core plugs. Note that the BVI shown in the figure may be smaller than the true value. This is because the acquisition of echo shape limits the minimum echo spacing. Even though we reduced our echo spacing to 1ms, the transient effects of the gradient pulse may still reduce our ability to measure short T1 components.

It is worthwhile to point out that the 1D T1MRI can also be applied to NMR logging to obtain high resolution T1 distribution. It is also straightforward to combine 1D MRI with T2 measurement using a CPMG sequence and gradient pulses to obtain 1D T2MRI distributions.

T1 Measurement with 2D Imaging

Applications of 2D NMR imaging include thin section imaging and full volume imaging. The thin section imaging gives a spatial fluid imaging at a specific axial position. The thickness of the slice is usually around few millimeters. The full volume imaging gives a spatial fluid distribution in a xy plane, which is an average over the whole length (z-axis). The resolution of the 2D imaging can go as good as 100μm. One must use short and long echo spacings to obtain relaxation weighted 2D imaging for determining free fluid and bound fluid volumes in the core plug. Combining the T1 measurements, we can obtain the pore size distribution associated with fluid distribution.

The experimental parameters used in our 2D T1MRI experiments are similar to the 1D T1MRI experiments. The hard 90° pulse was replaced by the Gaussian-shape soft pulse. The pulse length of the soft pulse was 2ms and there were 256 amplitude steps. During the soft pulse, a z-gradient was applied and its gradient strength was about 3 gauss/cm. The selected slice thickness was about 3 millimeters. The x-encode gradient and the readout gradient were about 14.6 gauss/cm and y-encode gradient varied from -1.9 gauss/cm to 1.9 gauss/cm with 64 steps. The length of both the x and y-encode gradient pulse was 1 ms and the dwell time acquisition was 4μs. Each echo was composed of 256 data points.

The data processing procedure of 2D T1MRI is also very similar to the 1D T1MRI except that we perform a 2D FFT before T1 inversion using BRD. During the FFT, we first smooth the

imaging by apodizing the spin echo train with a Lorenz lineshape that has a 500Hz linewidth. This apodization did not reduce spatial resolution very much, but reduce the noise significantly. In the T1 inversion, we selected 20 different T1 components from 3ms to 3s with equal step size in a logarithmic scale. Figure 6 shows the results of the 2D T1MRI of a core plug (referred as plug-A). The diameter of the core plug is about 1.5 inches and the length is about 2 inches. Its outward appearance is that of an intergranular sandstone/carbonate core plug. However, from the MRI imaging we learned that there are a few small vugs and a very large vug inside the core. The first image of the top row in Figure 6 is regular porosity distribution imaging. The second image shows the BVI distribution with 33ms T1 cutoff. The third image shows the free fluid distribution. The fourth and fifth images show geometric mean T1 images calculated from the whole T1 distribution and T1 distribution for BVI only, respectively. In order to show the T1 distribution with NMR imaging, we averaged every four images and used the geometric mean T_{1G} of the four T1 components as the T1 component of the averaged imaging. The five averaged imagings are shown at the bottom row of Figure 6.

Figure 6 gives a clear view of where the free fluid and irreducible water distributed in the core plug are. It is also very clear that T_{1G} values of the fluid imbedded in vugs are very similar to that of the free water which stayed on the surface of the core plug. The difference between short T1 imaging and long T1 imaging clearly shows that there is no clay or other solid in the vugs. We also see that in the big vug, the relaxation time of the fluid is not all the same. There may be some paramagnetic impurities at the lower right corner which causes the water to relax slightly faster than at the free water rate. Beside these interesting features about the vugs, the 2D T1MRI also reveals significant details about the spatial distribution of the pore space.

Diffusion Measurement with 1D Imaging

Measurement of diffusion coefficients has been applied to differentiate petrophysical properties such as viscosity, wettability, and irreducible saturations. These quantities are very important in reservoir simulation and production. Various 1D and 2D methods of using diffusion contrasts in fluids to measure petrophysical parameters have recently been proposed. These include NMR fluid typing methods (MRF [20] and GIFT [21]) and 2D NMR methods (diffusion editing [22] and relaxation-diffusion 2D [23]). Here we propose combining diffusion measurement with NMR imaging (DMRI) as a way to image saturation distributions of different fluids.

There are several ways to implement DMRI experiments. One example of a 1D version of DMRI pulse sequences is shown in Figure 3, which is derived from a Tanner stimulated echo sequence by adding a spin echo sequence with gradient encoding. However, at the early stage of the development we also used CPMG sequences inserted with gradient pulses between 180° RF pulses. The first two echo periods were used for diffusion evolution by varying the gradient strength while the third echo period was for MRI detection. We started with the three-cell sample and varied the diffusion gradient from 0 to 7 gauss. The gradient of the MRI detection was 7 gauss for all measurements. Because the magnetization decay rate caused by diffusion is mainly determined by the gradient strength and the length of the gradient pulse during diffusion

periods, we took the diffusion pulse length as the effective echo spacing to exclude the time used between RF and gradient pulses. The effective echo spacing was 32ms and therefore the total length of the diffusion period was 64ms. Using similar processing as 1D T1MRI, Figure 7 shows the correlation map of diffusion and 1D MRI of the three-fluid sample. Because the length of the diffusion period is much longer than the T1 relaxation time (20ms) of one of three fluids in the tube, one of fluid imagings cannot be observed in the figure. For the same reason, the intensity of the second fluid whose T1 is about 200ms is also reduced. However the diffusion coefficients measured by CPMG DMRI are very accurate. The maximum of the water peak appears at about $4x10^{-5}$cm/s while the crude oil is about 10 times less.

Figure 8 shows the correlation map of diffusion and 1D MRI of a core plug (Plug-B) with the pulse sequence shown in Figure 3. Here we have replaced the CPMG sequence with a Tanner sequence. The total diffusion period has been reduced to 30ms, however, we varied the diffusion gradient from 0 to 11.7 gauss. Because the plug was placed vertically in the magnet, some of the water in the plug drained to the bottom of the holder. This is why the peak intensity is high at one end of the plug. Secondly, the diffusion coefficient at the two ends appears larger than in the middle and the change is gradual. This may be related to the internal field gradient. Due to the susceptibility contrast between grains and pore fluids, the actual gradient of the fluid includes external and internal field gradients. The distribution of the internal field gradient along the axial direction is usually in a U-shape, that is, at the two ends the gradient reaches maximum and the minimum is in the middle of a core plug. Assuming that the external gradient is uniform, the total gradient is also in a U-shape. The apparent diffusion coefficient, D_a, becomes $D_a=D_o(G_t/G_E)^2$, where D_o is the bulk diffusion coefficient, G_t is the total gradient, and G_E is the externally applied gradient. If the total gradient field is larger than the external gradient, the apparent diffusion coefficient will be larger than the true diffusion coefficient. Furthermore, restricted diffusion effects can reduce the apparent diffusion coefficients by a time-dependent factor determined by the tortuosity and diffusion time [17]. In the long diffusion time limit, the factor is equal to the tortuosity. The third feature that appears in Figure 8 is that the diffusion coefficient varies quite dramatically in the middle of the plug although its geometric mean may be similar. This could be the result of either restricted diffusion or a variation in the internal field gradients in the porous media.

CONCLUSIONS

The main advantages of performing MRI measurements on a rock sample are that the method is non-destructive and that its signal directly comes from the fluids in the sample. MRI reveals the heterogeneity of the fluid distribution in a rock sample. Relaxometry of a rock sample gives indirect pore size distribution and has had great success in characterizing petrophysical properties in open-hole logging.

The T1MRI and DMRI techniques illustrate how the combination of relaxometry with MRI can characterize fluid and pore-size distributions in rock samples. The combination of imaging with relaxometry not only provides the proton population map in core samples but also incorporates information on the relaxation time and diffusion coefficient of the pore fluids. The encoding was

achieved by imposing a saturation recovery sequence for the T1 relaxation or a Tanner (or similar) sequence for the diffusion coefficient before the imaging pulsing sequences. Thus the NMR image can be processed to yield the normal proton population image with an extra dimension showing either the relaxation time or the diffusion coefficient distributions. This allows us to identify how the fluid is distributed within the core plug using the contrast in the diffusion coefficients, as well as the characteristics of the pore fabric using the T1 relaxation time distribution. It also provides a way to study the surface wettability in the spatial image of a core plug in future.

ACKNOWLEDGEMENTS

We wish to acknowledge the support and encouragement of ChevronTexaco management and their permission to publish the paper.

REFERENCES

1. Rothwell, W.P. and Vinegar, H.J., "*Petrophysical Applications of NMR Imaging*". Applied Optics. **24**(23): p. 3969 - 3972 (1985).
2. Packer, K., "*Oil Reservoir Rocks Examined by MRI*", in *Encyclopaedia of Nuclear Magnetic Resonance*. 1996, John Wiley & Sons: London. p. 3365-3376.
3. Chen, S., Yao, X., Qiao, J., and Watson, A., "*Characterisation Of Fractured Permeable Porous Media Using Relaxation Weighted Imaging Techniques*". Magnetic Resonance Imaging. **13**(4): p. 599-606 (1995).
4. Borgia, G., Bortolotti, V., and Fantazzini, P. "*Combined Magnetic Resonance Relaxation And Imaging For Quantitative Determination Of Matrix And Vugular Porosity In Carbonate Cores*". in *SPE Annual Technical Conference Proc.*, 751-756 (1998).
5. Al-Mugheiry, M.A., Issa, B., and P.Mansfield. "*Imaging Fluid Movements Through Sandstones, Sands and Model Glass-Bead Packs Using Fast NMR Imaging Techniques*". in *the 2001 SPE Middle East Oil Show and Conference*. Bahrain: March 17-20 (2001).
6. Chen, S., Qin, F., Kim, K., and Watson, A., "*NMR Imaging Of Multiphase Flow In Porous Media*". AICHE Journal. **39**(6): p. 925-934 (1993).
7. Dereppe, J., Moreaux, C., and Schenker, K., "*Chemical Shift Imaging Of Fluid Filled Porous Rocks*". Magnetic Resonance Imaging. **9**(5): p. 809-814 (1991).
8. Majors, P., Ping, L., and Peters, E., "*NMR Imaging Of Immiscible Displacements In Porous Media*". SPE Formation Evaluation. **12**(3): p. 164-169 (1997).
9. Bonalde, I., Martinlandrove, M., Benavides, A., Martin, R., and Espidel, J., J. Appl. Phys. **78**(10): p. 6033-6038 (1995).
10. Wassmuth, F., Green, K., and Randall, L., "*Details of In Situ Foam Propagation Exposed with Magnetic Resonance Imaging*". SPE Reservoir Engineering. **4**(2): p. 135-145 (2001).
11. Fisher, D., Espidel, J., Huerta, M., Randall, L., and Goldman, J., " *Use of Magnetic Resonance Imaging as a Tool for the Study of Foamy Oil Behaviour for an Extra-*

Heavy Crude Oil. T2 / Viscosity Correlation with Respect to Pressure". Transport in Porous Media. **35**: p. 189-204 (1999).

12. Straley, C., Rossini, D., Schwartz, M., Stromski, M., Hrovat, M., and Patz, S., "*Particle Filtration In Sandstone Cores: A Novel Application Of Chemical Shift Magnetic Resonance Imaging Techniques*". The Log Analyst. **36**(2): p. 42-51 (1995).
13. Zwagg, C., Stallmach, F., and Hanssen, J. "*Application Of NMR and CT- Analytical Methods To Assess The Formation Damage Potential Of Drilling Fluids*". in *International Symposium Of SCA Proc.*, 1-12 (1998).
14. Randall, L., Green, K., Fisher, D., Goldman, J., and Prichard, T. "*Strategy to reduce uncertainties in core analysis programs through the use of magnetic resonance imaging: a new perspective*". in *2002 International Symposium of the Society of Core Analysts*, SCA2002-36. Monterey, CA: September 22-25 (2002).
15. Sun, B. and Dunn, K.-J., "*Probing the internal field gradients in porous media*". Phy. Rev. E. **65**: p. 051309 (2002).
16. Dunn, K.-J., "*Enhanced Transverse Relaxation in Porous Media due to Internal Field Gradients*". Journal of Magnetic Resonance. **156**: p. 171–180 (2002).
17. Dunn, K.J., Bergman, D.J., and Latorraca, G.A., "*Nuclear Magnetic Resonance: Petrophysical and Logging Applications*". Handbook of Geophysical Exploration, Section I, Seismic Exploration,, ed. Treitel, K.H.S. Vol. 32. 2002, New York: Pergamon. 293.
18. Butler, J.P., Reeds, J.A., and Dawson, S.V., "*Estimating solutions of first kind integral equations with nonnegative constraints and optimal smoothing*". SIAM J. Numer. Anal. **18**: p. 381–397 (1981).
19. Tanner, J.E., "*Use of the Stimulated Echo in NMR Diffusion Studies*". J. Chem. Phys. **52**: p. 2523 (1970).
20. Freedman, R., Sezginer, A., Flaum, M., Matteson, A., Lo, S., and Hirasaki, G.J. "*A New NMR Method of Fluid Characterization in Reservoir Rocks: Experimental Confirmation and Simulation Results*". in *Society of Petroleum Engineers*. Dallas, TX (2000).
21. Sun, B. and Dunn, K.-J., "*NMR Inversion Methods for Fluid Typing*". IP.COM. **IPCOM000010000D**(08-Oct): p. 21 (2002).
22. Hurlimann, M.D. and Venkataramanan, L., "*Quantitative Measurement of Two-Dimensional Distribution Functions of Diffusion and Relaxation in Grossly Inhomogeneous Fields*". Journal of Magnetic Resonance. **157**: p. 31–42 (2002).
23. Sun, B. and Dunn, K.-J. "*Core analysis with two dimensional NMR*". in *2002 International Symposium of the Society of Core Analysts,* SCA2002-38. Monterey, CA: September 22-25 (2002).

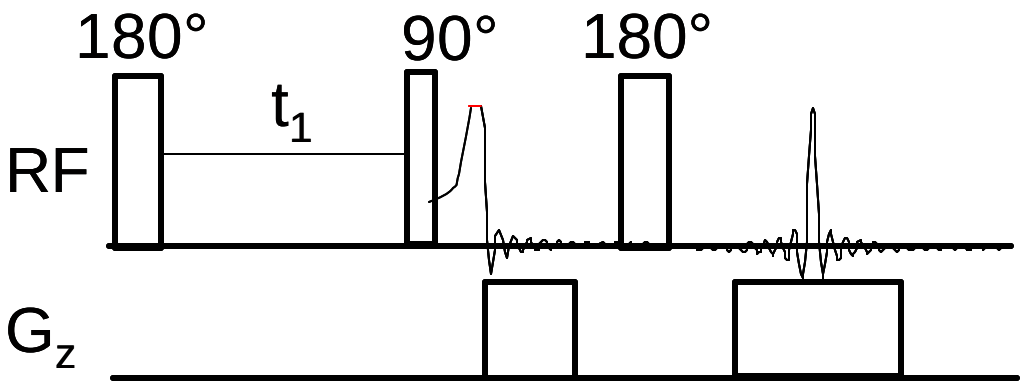

Figure 1. 1D version of a T1 MRI pulse sequence which is derived from an inversion-recovery sequence by adding a spin echo sequence with two pulsed gradients. The first gradient is for frequency/position encoding and the second, for readout of spatially encoded hydrogen. Variation of T1 recovery time t_1 yields T1 distributions of fluids in a rock sample.

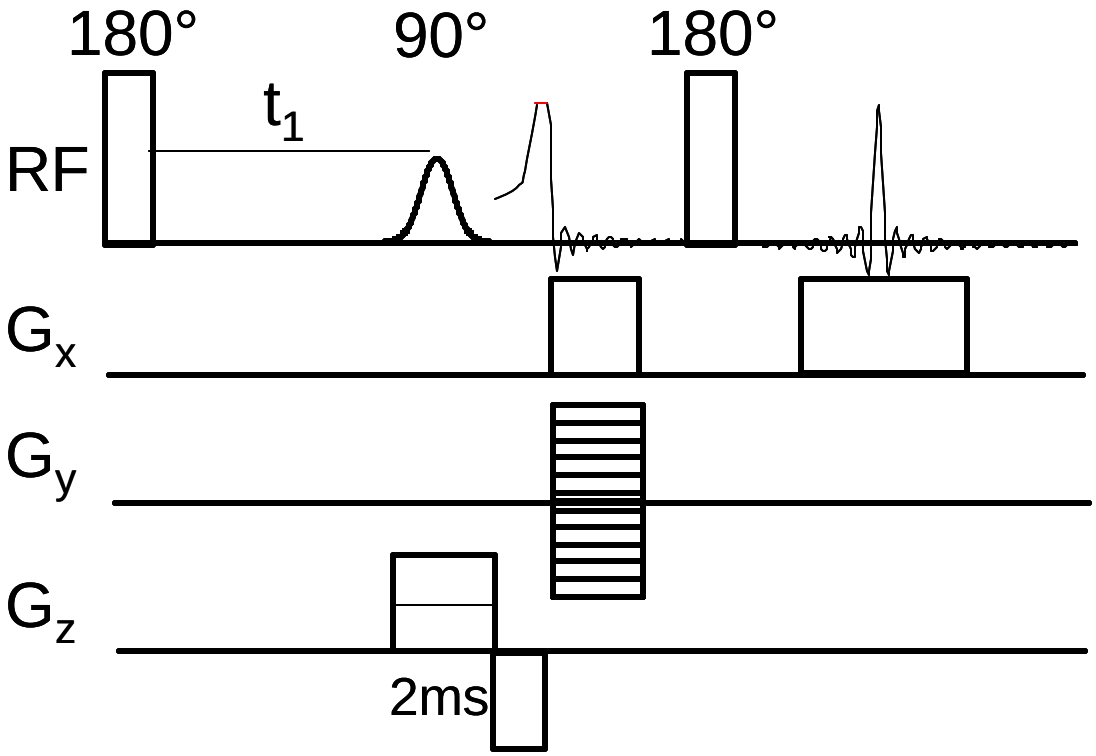

Figure 2. 2D version of a T1 MRI pulse sequence which is derived from an inversion-recovery sequence by adding a spin echo sequence with four pulsed gradients. The first G_x pulse is for frequency/position along the x-axis encoding, and the second G_x pulse, for readout of spatially encoded hydrogen. The G_y gradient is for encoding along the y-axis by varying its amplitude. The G_z pulse combined with the shaped RF pulse selects a xy slice. Variation of T1 recovery time t_1 yields T1 distributions of fluids in a rock sample.

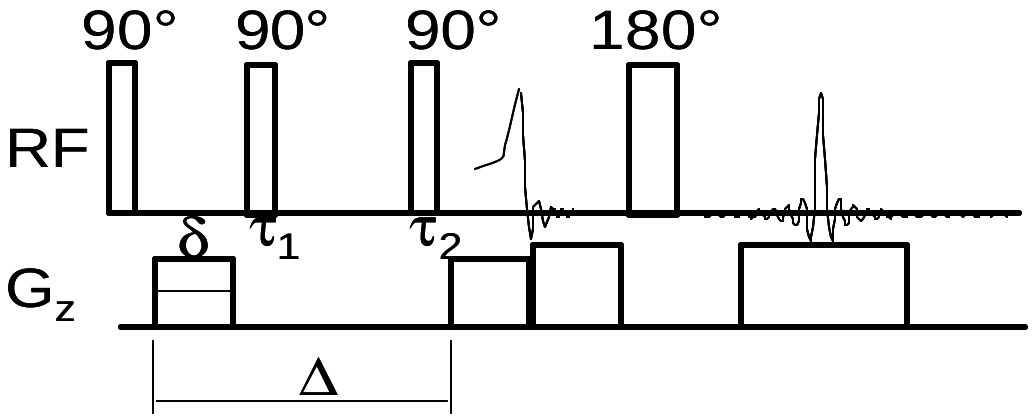

Figure 3 1D version of a Diffusion MRI pulse sequence which is derived from a Tanner stimulated echo sequence by adding a spin echo sequence with pulsed gradients. The first two gradients cause diffusion modulation on echo intensity. The third and fourth gradients are for obtaining imaging. The Variation of the first two gradient amplitude or time interval Δ (δ) yields distributions of diffusion coefficients in a rock sample.

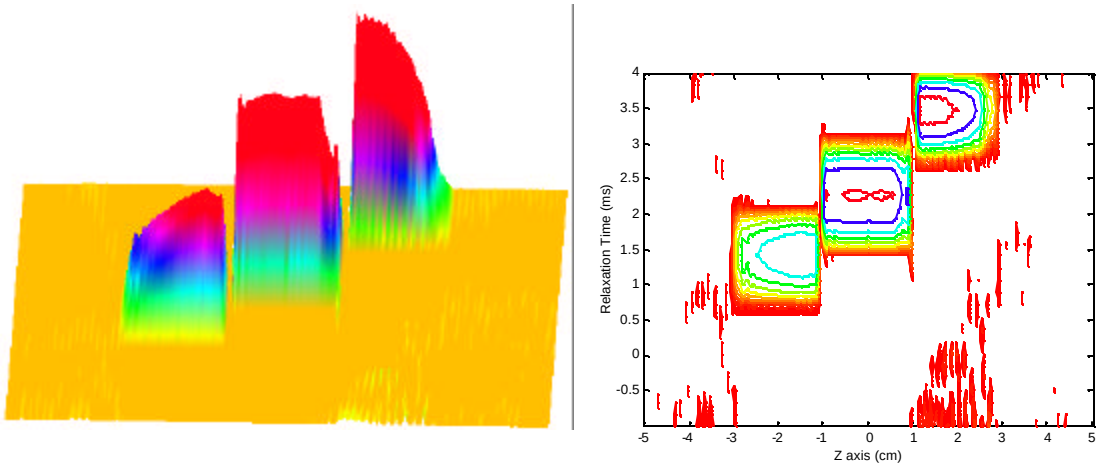

Figure 4. a 1D T1MRI correlation map of three 2cm long cells of different fluids: distilled water with T1 of 3s, crude oil of 200ms, and doped water of 20ms. Left is the 3D plot showing proton amplitude versus sample dimension and T1 relaxation time, while the right is the contour plot. Note that the intensity profiles of two cells at their ends are not flat due to end effects from the gradient coil.

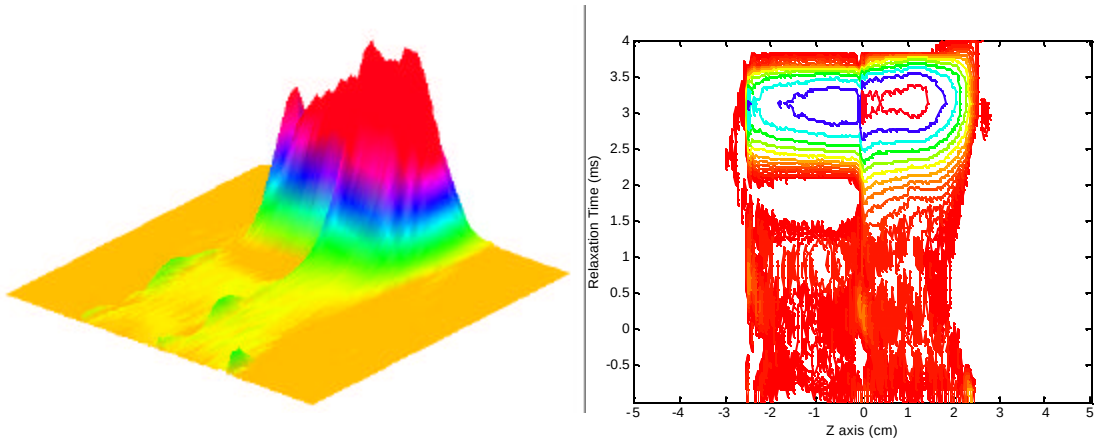

Figure 5. a 1D T1MRI correlation map of two sandstone plugs. Left is the 3D plot of proton amplitude versus sample dimension and T1, while the right is the contour plot.

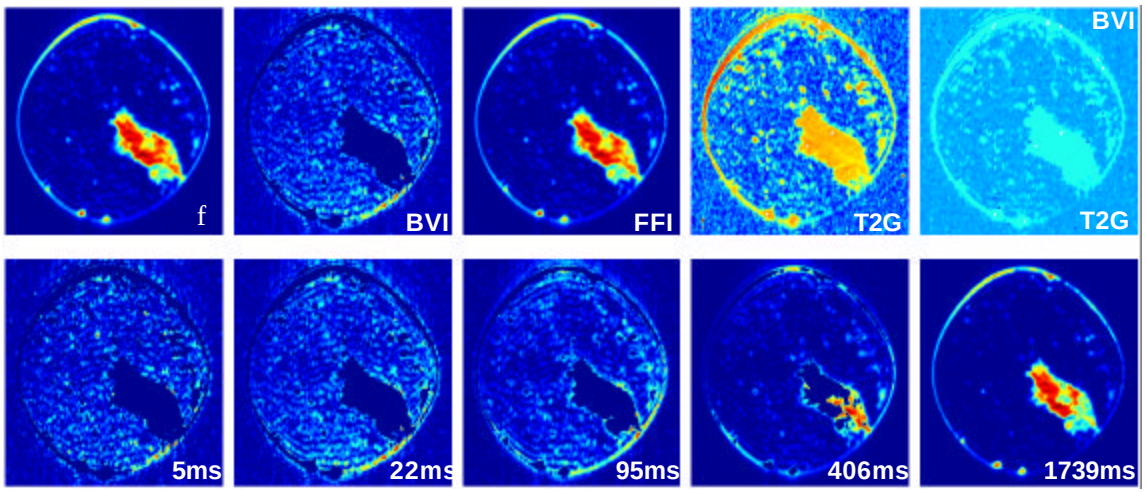

Figure 6. Results of 2D T1MRI of Plug-A: (top) porosity, BVI (with 33ms T1 cutoff), FFI, T1G, and T1G of BVI maps, and (bottom) five images at different T1 bins. Each T1 bin is an average of the adjacent four T1 imagings used in the BRD inversion. The diameter of the core plug is about 1.5 inches and the length is about 2 inches. Its outward appearance is that of an intergranular sandstone/carbonate core plug. The porosity imaging reveals a few small vugs and a very large vug inside the core.

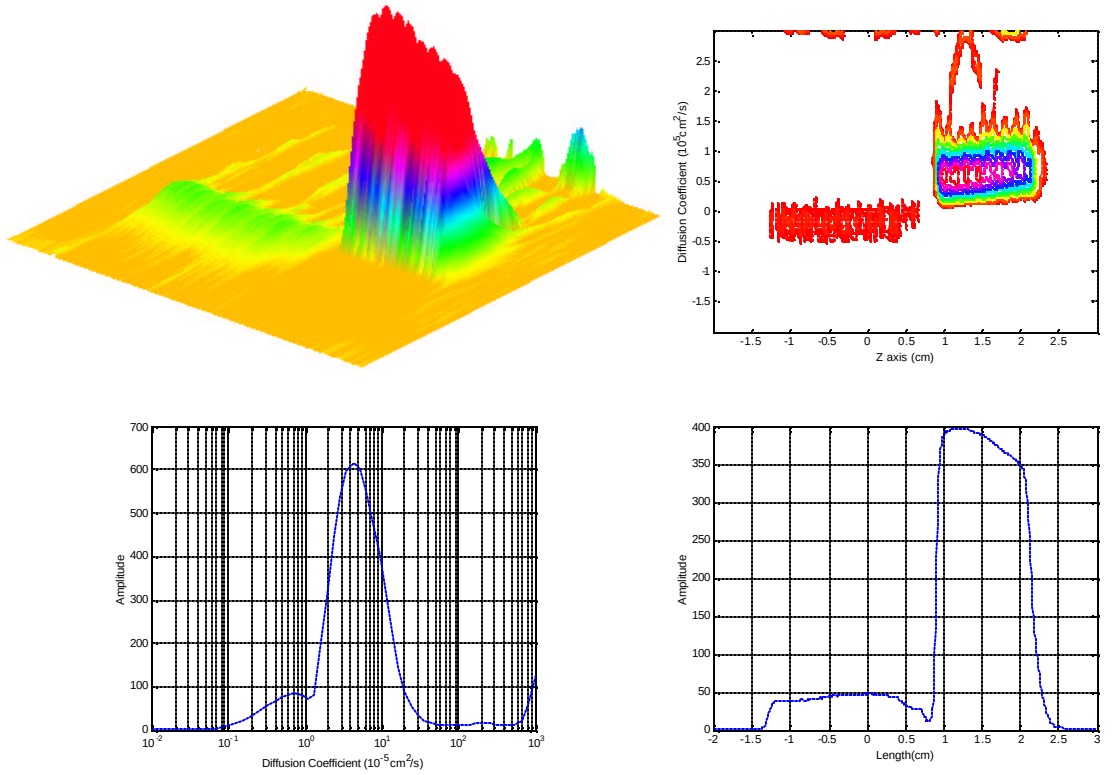

Figure 7 1D diffusion MRI spectra of a three-fluid sample. Top row shows the 3D plot of proton amplitude versus sample dimension and diffusion coefficient (left) and the contour plot (right). Bottom row is the projected diffusion distribution and axial signal profile. Note that the signal profile is not flat because some portions have short T1 components which were not observed due to long diffusion time.

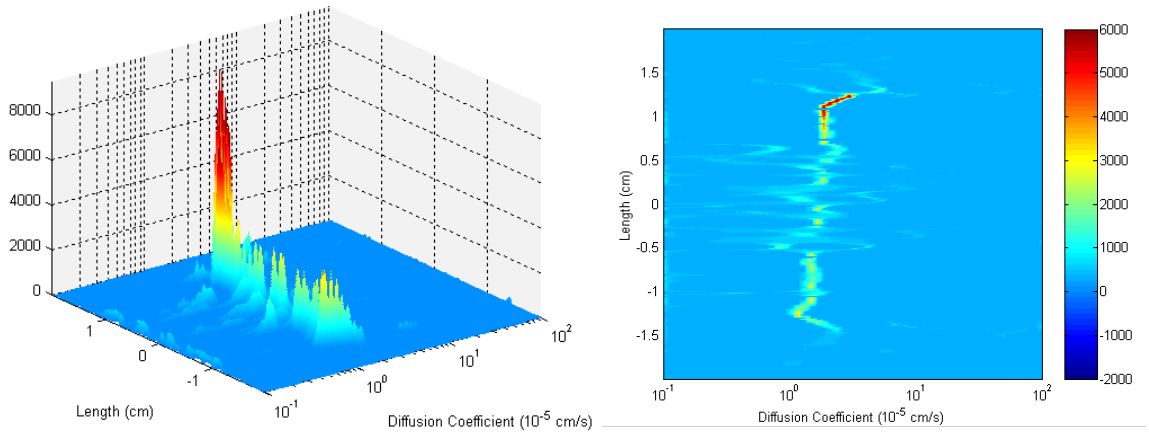

Figure 8. 1D diffusion MRI spectra of Plug-B measured by the pulse sequences shown in Figure 3. The diffusion coefficient varies quite dramatically in the middle of the plug although its geometric mean may be similar. This could be the results of either restricted diffusion or a variation in the internal field gradients in the porous media.